HHS Public Access

Author manuscript

Cell Rep. Author manuscript; available in PMC 2022 April 27.

Published in final edited form as:

Cell Rep. 2022 March 29; 38(13): 110605. doi:10.1016/j.celrep.2022.110605.

Neural readout of a latency code in the active electrosensory system

Krista E. Perks[1,2], **Nathaniel B. Sawtell**[2,3,*]

[1]Department of Biology, Wesleyan University, Middletown, CT 06459, USA

[2]Zuckerman Mind Brain Behavior Institute, Department of Neuroscience, Columbia University, New York, NY 10027, USA

[3]Lead contact

SUMMARY

The latency of spikes relative to a stimulus conveys sensory information across modalities. However, in most cases, it remains unclear whether and how such latency codes are utilized by postsynaptic neurons. In the active electrosensory system of mormyrid fish, a latency code for stimulus amplitude in electroreceptor afferent nerve fibers (EAs) is hypothesized to be read out by a central reference provided by motor corollary discharge (CD). Here, we demonstrate that CD enhances sensory responses in postsynaptic granular cells of the electrosensory lobe but is not required for reading out EA input. Instead, diverse latency and spike count tuning across the EA population give rise to graded information about stimulus amplitude that can be read out by standard integration of converging excitatory synaptic inputs. Inhibitory control over the temporal window of integration renders two granular cell subclasses differentially sensitive to information derived from relative spike latency versus spike count.

In brief

In many systems, information is conveyed by the precise latency of spikes relative to a sensory stimulus. Perks and Sawtell use intracellular recordings and modeling to reveal how such a latency code is read out by neurons in the active electrosensory system of fish.

Graphical Abstract

*Correspondence: ns2635@columbia.edu.

AUTHOR CONTRIBUTIONS

K.E.P. and N.B.S. conceived of the project and designed the experiments. K.E.P. performed the experiments, analyzed the data, and performed the modeling. K.E.P. and N.B.S. wrote the manuscript.

DECLARATION OF INTERESTS

The authors declare no competing interests.

SUPPLEMENTAL INFORMATION

Supplemental information can be found online at https://doi.org/10.1016/j.celrep.2022.110605.

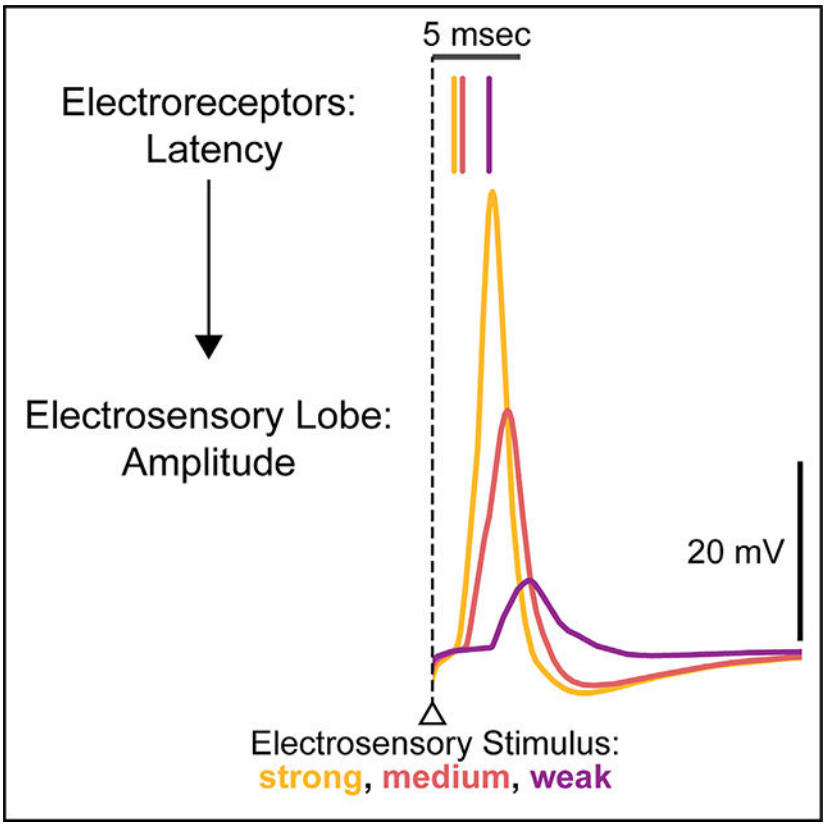

INTRODUCTION

The latency of spikes evoked by sensory stimuli convey information about non-temporal features (e.g., stimulus amplitude, location, or identity) at various processing stages across sensory modalities, including in vision (Gawne et al., 1996; Gollisch and Meister, 2008; VanRullen et al., 2005), audition (Ashida and Carr, 2011; Chase and Young, 2007; Furukawa and Middlebrooks, 2002; Grothe and Klump, 2000; Heil, 2004; Zohar et al., 2011), olfaction (Bathellier et al., 2008; Cury and Uchida, 2010; Shusterman et al., 2011), somatosensation (Johansson and Birznieks, 2004; Panzeri et al., 2001; Saal et al., 2016), and active electrosensation (Bell, 1990b; Hall et al., 1995; Szabo and Hagiwara, 1967). Latency codes have potential advantages over conventional rate codes in terms of speed (Gollisch and Meister, 2008; VanRullen et al., 2005), information capacity (Rieke et al., 1996; Theunissen and Miller, 1995), and energy efficiency (Lennie, 2003). Moreover, latency information appears to be sufficient for aspects of olfactory (Chong et al., 2020; Chong and Rinberg, 2018; Smear et al., 2011), tactile (Thomson and Kristan, 2006), and electrosensory (Hall et al., 1995) mediated behavior. However, unlike conventional spike rate codes, latency codes ostensibly require explicit postsynaptic readout mechanisms, the nature of which remains controversial (Stanley, 2013). Motor corollary discharge (CD) has been hypothesized to provide a central reference signal for reading out latency codes in cases in which sensory input is time locked to behavior (Bell, 1989; Crapse and Sommer, 2008; Moore et al., 2013; Shusterman et al., 2011). Alternatively, latency codes could be read out based on

information contained in the relative timing of spikes across a population of inputs (Haddad et al., 2013; Panzeri et al., 2014; Uchida et al., 2014; Zohar and Shamir, 2016).

The active electrosensory system of weakly electric mormyrid fish offers a number of advantages for examining how latency information is utilized by postsynaptic neurons. Mormyrid fish emit brief pulsed electrical fields known as electric organ electric discharges (EODs). Nearby objects with conductivity higher (lower) than the surrounding water increase (decrease) the amplitude of the EOD-induced field (Figure 1A). A-type mormyromast electroreceptors on the skin transduce increases (decreases) in the local amplitude of the EOD pulse into highly precise, smoothly graded decreases (increases) in spike latency (Bell, 1990b; Sawtell et al., 2006; Szabo and Hagiwara, 1967). Although most EAs also fire more spikes in response to EOD amplitude increases, evidence from intra-axonal recordings (Bell, 1990a), information theoretic analysis of EA responses (Bell, 1990b; Sawtell and Williams, 2008), and behavioral studies (Hall et al., 1995) suggest the functional importance of latency coding in this system. EAs project somatotopically to the hindbrain electrosensory lobe (ELL) where they form excitatory synapses predominantly with two anatomically distinct subclasses of interneurons known as deep and superficial granular cells (DGCs and SGCs) (Bell et al., 1989, 2005; Zhang et al., 2007) (Figure 1B). Granular cells send their axons to the superficial layers of the ELL where they synapse onto the output cells of the ELL and hence serve as an obligatory relay for electrosensory information (Bell et al., 2005). CD inputs related to the EOD motor command are prominent in the ELL and have been hypothesized to provide a reference signal that could serve to read out latency-coded input at the level of the ELL granular cells (Bell, 1989, 1990a; Hall et al., 1995) (Figure 1C). However, the small size and dense packing of granular cells has, until now, prevented *in vivo* recordings required to test this hypothesis.

RESULTS

Two physiologically distinct granular cell subclasses integrate EA and CD input

Granular cell responses were characterized using blind whole-cell recordings from the medial zone of the ELL in awake paralyzed fish (STAR Methods). In this preparation, neuromuscular paralysis blocks the EOD, but EOD motor commands continue to be emitted spontaneously by the fish at a rate of ~3–5 Hz, leaving CD input to the ELL intact. The EOD is mimicked by a brief electrical pulse delivered either at a brief (4.5 ms) delay relative to the EOD motor command, approximating normal conditions, or at a long (50 ms) delay. The former condition (termed short delay) is used to study the normally occurring interactions between electrosensory and CD inputs, while the latter (termed long delay) allows sensory and CD inputs to be observed separately.

Histological recovery of subset of recorded granular cells filled with biocytin revealed laminar locations and morphological properties consistent with previous anatomical descriptions of DGCs and SGCs (Bell et al., 2005; Zhang et al., 2007) (Figure 2A). We report exclusively on subthreshold responses because somatically recorded action potentials were small and often difficult to distinguish, likely due to an electrotonically remote site of initiation at the distal end of a thin initial segment (Bell et al., 2005; Zhang et al., 2007). Electrosensory stimulation evoked short-latency synaptic excitation in both DGCs

and SGCs, consistent with monosynaptic input from EAs. Excitation in DGCs was sharply peaked and appeared to be truncated by inhibition (Figures 2B and 2D, *gray arrow*), while excitation in SGCs decayed much more slowly (Figures 2C and 2D). Prior electron microscopy and *in vitro* studies indicate that GABAergic interneurons, known as large multipolar intermediate layer (LMI) cells, form inhibitory synapses onto granular cells (Han et al., 2000; Meek et al., 2001; Zhang et al., 2007).Differences in the time course of electrosensory responses in DGCs and SGCs may reflect differences in the strength of LMI-mediated inhibition.

The possibility that granular cells receive CD input related to the EOD motor command has been suggested based on prior work but not directly shown (Bell, 1990a). Our intracellular recordings confirmed prominent CD input to granular cells. DGCs exhibited highly stereotyped, short-latency excitation time-locked to the EOD motor command (Figures 2E, 2G, and S1). In some DGCs, CD excitation appeared to be truncated by inhibition (see Figure 3C, *black trace*), similar to their responses to electrosensory input. In contrast, SGCs typically exhibited a stereotyped, short-latency hyperpolarization followed by a depolarization (Figure 2F, 2G, and S1). At more hyperpolarized potentials, CD responses consisted mainly of a depolarization(Figure 2F, *inset, gray arrows*), suggesting that CD input to SGCs is comprised of synaptic inhibition followed by excitation. Prior studies suggest that CD input to the ELL originates from the medial juxtalobar nucleus (JLm) (Bell and von der Emde, 1995; Mohr et al., 2003). Consistent with this, electrical microstimulation in the vicinity of the JLm evoked synaptic responses resembling naturally occurring CD responses, including short-latency depolarizations in DGCs and hyperpolarizations in SGCs (Figure S1). However, since JLm neurons are thought to be glutamatergic (Bell and von der Emde, 1995; Mohr et al., 2003), the origin of CD-inhibition in SGCs is unclear.

CD input enhances but is not required for reading out EA input to granular cells

Next we characterized granular cell responses to modulations of electrosensory stimulus amplitude. Such modulations mimic increases and decreases in EOD amplitude due to conducting and nonconducting objects, respectively (STAR Methods). To test the role of CD input, we compared granular cell responses evoked by electrosensory stimuli delivered at short (naturally occurring) versus long delays relative to the EOD command. In both conditions, increases in electrosensory stimulus amplitude led to decreases in postsynaptic response onset in granular cells (Figures 3A–3C, and 3G), as expected based on well-characterized latency shifts in EAs (Bell, 1990b; Szabo and Hagiwara, 1967). Large graded changes in postsynaptic response amplitude (>10 mV) were observed in response to stimuli presented at both short and long delays (Figures 3A–3C, 3H, and 3I). These findings are consistent with the hypothesis that latency coded EA input induces changes in postsynaptic response amplitude in granular cells but suggest that CD input is not required for this transformation.

To further evaluate the effect of CD input, we compared measured granular cell responses to those calculated based on a linear sum of the granular response to electrosensory stimuli delivered at a long delay and the response to the CD input alone (Figures 3D–3F, *dashed line*). Most SGCs exhibited supralinear summation of electrosensory and CD input,

particularly at high stimulus amplitudes (Figures 3A, 3D, 3H, and S2). The enhancement of sensory-evoked depolarizations in SGCs is notable given that SGCs typically exhibited CD-evoked inhibition (Figures 3A and S2). Supralinear summation was not observed between CD input and EPSP waveforms generated by somatic current injections in SGCs (Figure S2), suggesting that facilitatory interactions between CD and EA input might occur electrotonically distant from the soma in the long, thin dendrites of SGCs (Bell et al., 2005; Zhang et al., 2007). More varied interactions between CD and electrosensory inputs, including both supralinear (Figures 3B and 3E) and sublinear (Figures 3C and 3F) summation, were observed in DGCs. Sublinear summation is expected for cells, like the example shown in Figure 3C, in which CD excitation is followed by inhibition. On average, DGC responses were modestly enhanced by CD input (Figure 3I).

Finally, we recorded subthreshold responses to modulations of electrosensory stimulus amplitude in E-type output cells of the ELL, one of the major postsynaptic targets of granular cells (Bell et al., 2005; Grant et al., 1996). Responses of E cells resembled those of granular cells in that long delay electrosensory stimuli evoked graded changes in subthreshold response magnitude that were enhanced when stimuli were delivered at the natural delay relative to the EOD motor the command (Figure S3). Overall, these results argue against the hypothesis that CD is required for reading out electrosensory input, but are consistent with a role for CD in enhancing or “gating-in” responses to the fish’s own EOD (Meyer and Bell, 1983).

Diverse spike latency and number tuning in EAs

Granular cells pool excitatory input from an estimated 4–7 EAs innervating nearby electroreceptors on the skin (Bacelo et al., 2008; Bell, 1990a). To determine the potential implications of such convergence for reading out electrosensory input, we obtained intracellular recordings from EAs in the granular layers of the ELL near their central terminals. Responses to identical electrosensory stimuli were obtained from 7–21 individual EAs in each of four fish. Recording locations were restricted to the same somatotopic region of the ELL to minimize potential response variability due to electroreceptor location on the skin. All EAs exhibited smoothly graded decreases in spike latency with increases in stimulus amplitude and most also exhibited increases in spike number (Figures 4A–4C), consistent with prior studies (Bell, 1990b; Sawtell et al., 2006; Szabo and Hagiwara, 1967). Although responses were highly reliable across repeated trials within individual EAs, substantial heterogeneity was observed in latency tuning across the population (Figures 4A–4C). To quantify this, we fit exponential functions to first spike latency-stimulus amplitude response curves for all recorded EAs (Figure 4D) and plotted the distribution of parameters for each fish (Figures 4E–4G). Substantial heterogeneity was observed across EAs within each fish in terms of the sensitivity of latency shifts to stimulus amplitude (decay), the total range of latency shifts (amplitude), and the minimum first spike latency (offset). To isolate effects of relative latency shifts from recruitment, we identified the range of stimulus amplitudes over which EAs fire at least one spike (Figure 4H, gray box).

Because first spike latencies converge onto a minimum value, presumably set by biophysical limits, heterogeneous latency tuning results in a stimulus-dependent decrease in the interval

between first spikes across the population (Figure 4H). This implies that a rate code for stimulus amplitude exists at the level of the input population even when the total number of EA spikes remains constant.

EAs also exhibited diversity in their spike count tuning (Figures 4A–4C). Consistent with prior results, second and subsequent spikes followed earlier spikes by a fixed offset (Figure 4I) (Bell, 1990b; Sawtell et al., 2006). Notably, the number of spikes fired by an individual EA appeared unrelated to its first spike latency tuning. To demonstrate that the maximum number of spikes in an EA's response is not simply predicted by its first spike's latency, we compared the actual distribution of the number of spikes fired by EAs at the maximum stimulus amplitude (Figure 4J, *red*) to the distribution of the number of spikes predicted by adding subsequent spikes at the experimentally determined offsets from each EA's first spike (Figure 4J, *black*) (see STAR Methods for more detail on how this condition was simulated; same as in Figures 5E–5H, orange). Recorded EAs exhibited a broader distribution of total spikes than expected based on the simulation, suggesting that spike latency and spike count tuning vary independently within EAs. Comparing the median EA spike count as a function of stimulus amplitude for recorded versus simulated populations suggests that this independent tuning results in spike count grading over a wider range of stimulus amplitudes (Figure 4K).

Postsynaptic readouts in SGCs and DGCs based on EA convergence

The foregoing results suggest that the EA population contains graded information about stimulus amplitude that could be read out based on simple input summation in granular cells independent of a fixed reference signal. To test this, we constructed conductance-based model neurons with parameters adjusted to match the rise and decay of near-threshold EPSPs recorded in SGCs and DGCs (Figure S4). Input to the model consisted of spikes from four EAs randomly subsampled from the recorded population. Though we chose to focus on simplified models to gain insight into the functional significance of EA convergence, numerous additional factors may contribute to measured subthreshold responses in granular cells, e.g., mixed chemical and electrical synapses between EAs and granular cells and voltage-gated conductances (Zhang et al., 2007). Responses in model cells receiving only excitatory EA input were broad in duration and exhibited large, graded increases in peak depolarization as a function stimulus amplitude, similar to recorded SGCs (Figures 5A and 5B). To mimic the brief electrosensory responses exhibited by DGCs, we added strong inhibitory input at a short delay (2–4 ms) after the onset of the excitatory response, effectively truncating the time window for integrating EA input. Model responses were much briefer under these conditions, resembling recorded DGCs, but still exhibited large, graded increases in peak depolarization as a function stimulus amplitude (Figures 5C and 5D). Aside from changes in the absolute magnitude of responses, results were similar over a range of values for EA input number and inhibitory input delay (Figure S4). These results suggest that granular cell responses to electrosensory stimuli observed *in vivo* can largely be explained based on convergence of a small numbers of excitatory EA inputs and, for DGCs, sensory-evoked inhibition.

Next, we used the model to test the respective contributions of diversity in latency versus spike count tuning in EAs to postsynaptic responses in granular cells. Model SGC and DGC responses to subsampled EA inputs were compared for three sets of manipulated EA inputs in which (1) diversity in both latency and spike count tuning was eliminated; (2) diversity in latency tuning was eliminated but diverse spike count tuning remained intact; and (3) diversity in spike count tuning was eliminated but diverse latency tuning remained intact (STAR Methods). These four sets of input are illustrated in Figure 5E. In the absence of diverse latency tuning, the EA population inter-spike-interval is approximately the same across stimulus amplitudes. Similarly, in the absence of diverse spike count tuning, most EAs fire a maximal number of spikes even at relatively low stimulus amplitudes. Consistent with this, removal of diversity in both latency tuning and spike count tuning resulted in postsynaptic responses that were near maximal across a wide range of stimulus amplitudes for both SGCs and DGCs (Figures 5F–5H, blue).

The relative importance of diversity in latency tuning versus diversity in spike count tuning depended on the temporal window of postsynaptic integration as set by the timing of inhibition (Figure S4). When inhibition onset was rapid, removing diversity in latency tuninghad the major impact onmodel responses (Figure 5F, purple). In the absence of inhibition, removing diversity in spike count tuning had the major impact on model responses(Figure 5G, orange). For intermediate values of inhibition delay, graded responses could be supported by either diversity in latency tuning or spike count tuning (Figure 5H). These results suggest that narrower versus wider temporal integration windows render DGCs and SGCs differentially sensitive to information contained in the relative timing versus the overall number of EA spikes, respectively. Sensitivity of peak response amplitude to the relative timing of EA inputs can be explained by powerful sensory-evoked inhibition and steep rising sensory-evoked excitation (both notable features of DGCs). Assuming that inhibition is triggered by the first EA input to a granular cell (see discussion), a decrease in the relative timing of subsequent EA inputs will result in the postsynaptic response reaching a more depolarized level before being truncated by inhibition (Figure 5I).

Comparing ELL zones provides additional evidence for the importance of diverse EA tuning

Given that some degree of heterogeneity in response properties across a neuronal population is inevitable, we sought further evidence that diverse EA tuning represents a functional specialization. In addition to the EAs studied here (termed A-type), mormyrid fish also possess additional B-type receptors sensitive to object-induced changes in both the amplitude and shape of the EOD waveform (von der Emde and Bleckmann, 1992, 1997). B-type EAs project to granular cells located within an adjacent region of the ELL known as the dorsolateral zone (DLZ) (Bell et al., 1989). Although circuitry, cell types, and CD input appear generally similar between the medial zone (MZ) and DLZ, prior work has shown that spike threshold is highly uniform across B-type EAs (Bell, 1990b). If diverse tuning is essential for the postsynaptic readout of information conveyed by A-type EAs, the absence of such diversity in B-type EAs would be expected to manifest as differences in postsynaptic responses in the MZ versus the DLZ.

As an initial test of this hypothesis, we compared field potential responses evoked by identical modulations of electrosensory stimulus amplitude for series of closely spaced electrode penetrations that passed through somatopically aligned regions of the MZ and the DLZ. The early negative component of such field potentials reflects excitation in the granular layer evoked by EAs innervating a small region of the skin (Bell et al., 1992; Gomez et al., 2004; Grant et al., 1998; Sawtell and Williams, 2008). In the MZ, field potential onset latency decreased while the amplitude exhibited prominent grading as a function of stimulus amplitude (Figure 6A). Such amplitude grading can be understood in the same terms as granular cell postsynaptic responses, i.e., as due to an increase in the summed input of a local population of EAs. In the DLZ, field potential onset latency also decreased; however, the amplitude of the field potential exhibited little grading as a function of stimulus amplitude (Figure 6B). To confirm that the difference in response amplitude changes across zones was not due to differences in overall sensitivity to sensory input, we plotted peak field potential amplitude as a function of peak latency across stimulus amplitude (Figures 6C–6F). The slope of this relationship was about four times greater in MZ compared with DLZ, though the range of latency shifts was similar (Figures 6F–6H). We hypothesize that the weaker amplitude grading in the DLZ is due to homogeneous response properties of B-type EAs, similar to the results obtained in the model with simulated EA populations lacking diverse tuning. These results further support the functional importance of diverse tuning in A-type EAs and motivate future studies of the postsynaptic readout of B-type EA input in the granular cells of the DLZ.

DISCUSSION

Compared with the many studies characterizing the encoding of sensory information by spike latency shifts, there have been relatively few tests of whether and how such information is actually utilized by postsynaptic neurons. The active electrosensory system is advantageous in this regard because latency decoding is hypothesized to occur in granular cells located just one synapse from the sensory periphery. In addition, central reference signals hypothesized to perform the decoding can be easily monitored and manipulated *in vivo*. However, until now, their small size and dense packing have precluded *in vivo* recordings from individual granular cells. Using *in vivo* whole-cell recordings we demonstrate that granular cells exhibit large stimulus-evoked changes in postsynaptic response amplitude, consistent with prior hypotheses that latency shifts in EAs are transformed into changes in response amplitude (Bell, 1990a). Although granular cells integrate EA input with motor CD signals providing a precise reference signal related to stimulus onset, such signals appear to gate or enhance responses rather than being strictly required to decode sensory input. Instead, we find that diverse latency and spike count tuning across the EA population gives rise to graded information about stimulus amplitude in the form of a rate code. Modeling indicates that sensory-evoked postsynaptic responses in two distinct subclasses of granular cells can be explained, without a fixed reference signal, simply by summation of excitatory input from a small number of converging EA inputs. Finally, a brief integration window set by powerful sensory-evoked inhibition renders DGCs highly sensitive to information contained in the relative latency of EA spikes, while the absence of strong inhibition renders SGCs more sensitive to total spike count.

Comparison to latency readout schemes proposed for other systems

One common proposal for reading out latency codes relies on fixed reference signals related to stimulus onset. CD signals are hypothesized to provide a reference signal for reading out latency codes in systems where the timing of sensory input is determined by the behavior of the animal (Crapse and Sommer, 2008; Cury and Uchida, 2010; Hall et al., 1995; Smear et al., 2011), for example saccades in vision, sniffing in olfaction, active touch in somatosensation, or the EOD in electrolocation. Alternatively, fixed reference signals could be contained in the sensory input itself, for example, by subsets of sensory neurons with short, stereotyped response latencies (Brasselet et al., 2012; Chase and Young, 2007; Gollisch and Meister, 2008). Other readout schemes rely on postsynaptic specializations such as specialized learning rules for tuning synaptic strength (Gutig and Sompolinsky, 2006; Thorpe et al., 2001) or competitive interactions mediated by recurrent inhibition (Haddad et al., 2013; Stern et al., 2018; Zohar and Shamir, 2016). The present findings are notable in that no fixed reference signal is required. Furthermore, diverse tuning across sensory input populations has been reported in numerous systems (see Bale et al., 2013; Goldberg, 2000; Raman et al., 2010), suggesting that the mechanism described here may be of general relevance for understanding how latency codes are utilized by the brain. In the mammalian auditory system, for example, there is wide variation in the sensitivity of auditory nerve fibers that co-varies with spontaneous firing rate, axonal morphology, and transcriptional patterns, and has been functionally linked to the wide dynamic range of human hearing (Liberman, 1982; Liberman and Oliver, 1984; Petitpre et al., 2018; Viemeister, 1983; Winter et al., 1990).

Although the origin of the diverse tuning observed across A-type electroreceptors is not known, a prior electrophysiological study noted that A-type electroreceptors exhibit widely varying spike thresholds, and an electron microscopy study observed notable variation in the area of the outer membrane of A cells (Bell, 1990b; Bell et al., 1989). Differences in types, distributions, or densities of voltage-gated channels across A-type electroreceptor cells or their afferent fibers have not been investigated but could also contribute to diverse responses. Another question for future studies is whether convergence of A-type EAs onto granular cells is random (as in our model) or subject to some forms of tuning or optimization. Although we did not systematically examine non-random connectivity, certain rules might be expected to enhance postsynaptic responses. For example, convergence of EAs with intersecting latency tuning curves is expected to give rise to non-monotonic postsynaptic responses (i.e., maximal responses at the intersection point). Response grading could potentially be enhanced if granular cells avoided pooling such EAs.

Implications for active electrosensory processing

The observation that precise central reference signals are present in granular cells raises the question of what advantages, if any, are conferred by the readout scheme proposed here. In contrast to the fixed temporal window provided by CD, sensory-evoked inhibition in DGCs provides a window for reading out relative latency information that shifts along with the sensory input. This may provide a means for maintaining sensitivity to small latency shifts, such as those due to prey (Gottwald et al., 2018), superimposed on larger shifts due to the animals' own behavior or large environmental features (Chen et al.,

2005; Sawtell and Williams, 2008; Sawtell et al., 2006). Anatomical studies have shown that the myelinated dendrites of LMI cells form large GABAergic synapses onto granular cells. LMI dendrites lack conventional synaptic inputs and are hypothesized to be activated directly by depolarization within granular cells via ephaptic coupling (Han et al., 2000; Meek et al., 2001). This unusual synaptic organization appears well-suited to mediate the rapid and powerful inhibition observed in DGCs. Whereas DGCs, LMI cells, and latency coding in EAs appear to be specializations of the active electrosensory system (all three are absent from an adjacent zone of the ELL that subserves the more evolutionarily ancient passive electrosense), SGCs are found in both systems (Bell et al., 2005). Based on our finding that SGCs are mainly sensitive to spike count while DGCs are sensitive to input timing, it is tempting to speculate that DGCs and LMIs are adaptations for utilizing temporal information associated with the evolution of the active electrosense. More broadly, our results are consistent with key roles for inhibition in temporal processing suggested by studies of a wide range of sensory systems, including olfaction, audition, and electrocommunication (Grothe, 2003; Heil, 2004; Lyons-Warren et al., 2013; Uchida et al., 2014). Finally, encoding stimulus amplitude independent of CD could enable a dual role for the active electrosensory system in utilizing information derived from the EODs of other fish. Consistent with such a function, one prominent close-range electrocommunication behavior, the echo response, has been suggested (though not yet proven) to be triggered by activation of mormyromast electroreceptors (Russell et al., 1974).

Limitations of the study

An important limitation of the present study was our inability to reliably measure the spiking output of granular cells. Similar difficulties were noted in a prior *in vitro* study and likely reflect a spike initiation site electrotonically remote from the soma (Bell et al., 2005; Zhang et al., 2007). Issues related to recording quality (e.g., filtering due to high access resistance) are unlikely, as synaptic responses in DGCs were both large and extremely rapid. Moreover, granule cells of the eminentia granularis (comparable in size to ELL granular cells) recorded in the same preparation with identical methods routinely exhibit overshooting action potentials (Kennedy et al., 2014; Sawtell, 2010). Spike threshold, as well as additional postsynaptic non-linearities, could enhance sensitivity to small changes in EOD amplitude. Nevertheless, the observation that subthreshold responses to electrosensory stimuli in E-type output cells were similar to those in granular cells support our conclusions that CD enhances, but is not required for, encoding electrosensory stimulus amplitude (Figure S3). A second limitation relates to the use of spatially uniform electrosensory stimulation. These simple stimuli greatly facilitated quantitative comparisons, which would have been difficult with local stimuli given the difficulty of maintaining stable recordings from small granular cells while mapping receptive fields. However, they obviously restricted us from studying potentially important effects of the spatial structure of electrosensory input. Due to the inherent blur in electrical images, EAs converging onto a given granular cell probably convey similar signals. However, LMIs likely receive electrosensory input from large regions of the body surface and may perform spatial computations such as lateral inhibition (Han et al., 2000; Meek et al., 2001). Given the apparent differences in sensory-evoked inhibition between DGCs and SGCs, these two sub-classes may differ not only in the temporal profiles of their sensory responses but also in their spatial tuning. Additional

key questions relate to synaptic and functional connectivity patterns linking granular cells to the rest of the ELL. While both DGCs and SGCs send axons to the superficial layers of the ELL where they contact several anatomically and functionally distinct neuronal subclasses, the details of their connectivity patterns are not known (Hollmann et al., 2016; Meek et al., 1999).

STAR★METHODS

RESOURCE AVAILABILITY

Lead contact—Further information and requests for resources and reagents should be directed to and will be fulfilled by the lead contact, Nathaniel Sawtell (ns2635@columbia.edu).

Materials availability—This study did not generate new unique reagents.

Data and code availability

- Raw and processed data have been deposited on G-Node: https://doi.org/10.12751/g-node.suibcf and are publicly available as of the date of publication.
- All original code has been deposited on G-Node: https://doi.org/10.12751/g-node.suibcf and is publicly available as of the date of publication.
- Any additional information required to reanalyze the data reported in this paper is available from the lead contact upon request.

EXPERIMENTAL MODEL AND SUBJECT DETAILS

Animals—Male and female wild-caught Mormyrid fish of the species *Gnathonemus petersii* were used in these experiments (fish were 7–12 cm in length, of unknown age, and sex was not specifically selected for). Fish were housed in 60 gallon tanks in groups of 5–20. Water conductivity was maintained between 70 and 150 microsiemens both in the fish's home tanks and during experiments. All experiments performed in this study adhere to the American Physiological Society's Guiding Principles in the Care and Use of Animals and were approved by the Institutional Animal Care and Use Committee of Columbia University.

METHOD DETAILS

Surgical procedures—For surgery to expose the brain for recording, fish were anesthetized (MS:222, 1:25,000) and held against a foam pad. Skin on the dorsal surface of the head was removed and a long-lasting local anesthetic (0.75% Bupivacaine) was applied to the wound margins. A plastic rod was cemented to the anterior portion of the skull to secure the head. The posterior portion of the skull overlying the ELL was removed. The valvula cerebelli was reflected laterally to expose the eminentia granularis posterior and the molecular layer of the ELL, facilitating whole-cell recordings. Gallamine triethiodide (Flaxedil) was given at the end of the surgery (~20 μg/cm of body length) and the anesthetic was removed. Aerated water was passed over the fish's gills for respiration. Paralysis blocks the effect of electromotoneurons on the electric organ, preventing the EOD, but the motor

command signal that would normally elicit an EOD continues to be emitted at an average rate of 2–5 Hz.

Electrophysiology—The EOD motor command signal was recorded with a Ag-AgCl electrode placed over the electric organ. The command signal is the synchronized volley of electromotoneurons that would normally elicit an EOD in the absence of neuromuscular blockade. The command signal lasts about 3 msec and consists of a small negative wave followed by three larger biphasic waves. Onset of EOD command was defined as the negative peak of the first large biphasic wave in the command signal.

For *in vivo* whole-cell recordings, electrodes (8–15 MΩ) were filled with an internal solution containing, in mM: K-gluconate (122); KCl (7); HEPES (10); Na2GTP (0.4); MgATP (4); EGTA (0.5), and 0.5%–1% biocytin (pH 7.2–7.4, 280–315 mOsm). No correction was made for liquid junction potentials. Only cells with stable membrane potentials more hyperpolarized than −45 mV were analyzed. Membrane potentials were recorded and filtered at 3–10 kHz (Axoclamp 2B amplifier, Axon Instruments) and digitized at 20–40 kHz (CED micro1401 hardware and Spike2 software; Cambridge Electronics Design, Cambridge, UK). *In vivo* local field potentials in Figure 6 were made with low resistance (<5MOhm) glass microelectrodes filled with 2 M NaCl.

Electrosensory stimulation—The EOD mimic was a 0.2 msec duration monophasic square pulse delivered between an electrode in the stomach and another positioned near the electric organ in the tail. In between recordings, the EOD mimic was presented at a baseline amplitude of 350 mA (stomach electrode negative) at the output of the stimulus isolation unit. To characterize neural tuning curves, stimulus amplitude was varied from +40% to −40% from the baseline amplitude. Specifically, the following shifts from baseline amplitude (as percent of baseline) were presented in pseudo-random order: −40, −30, −20, −10, −5, 0, +5, +10, +20, +30, and +40 (note that for the data presented in Figure 6, this range was reduced to −30% to +30% with 5% increments). To characterize interactions between electrosensory and corollary discharge inputs, responses were compared across conditions in which the EOD mimic was presented at a delay of either 50 msec (long delay) or 4.5 msec (short delay) following the EOD command.

Medial juxtalobar nucleus stimulation—The precise location of the medial juxtalobar nucleus (JLm) was determined by monitoring corollary discharge-evoked field potentials with extracellular recording electrodes. Low resistance, broken-tip glass capillary microelectrodes filled with 3 M NaCl were used for recording field potentials and for electrical stimulation of the JLm (stimulus duration was a single square wave pulse with a duration of 200 microseconds). The electrodes were directed at angles of about 45° with respect to the mid-sagittal plane and with a slight posterior to anterior direction. With the valvula reflected, entry points for the electrode tracks were just dorsal to the anterior tip of the exposed electrosensory lobe molecular layer. The corollary discharge-driven field potential characteristic of the JLm was recorded in such tracks at depths of 800–1500 microns below the surface (depending on fish size and exact tilt). Prior to searching for and recording granular cells, JLm electrode placement was confirmed by the ability of a near-threshold stimulus to evoke characteristic field potential responses in the granular

layers of ELL (Mohr et al., 2003). Minimum stimulus thresholds for evoking responses in ELL were 2–4 uA. For evoking responses in granular cells, a near threshold stimulus of 5uA was used.

Histology and morphological reconstructions—After recording, fish were deeply anesthetized with a concentrated solution of MS:222 (1:10,000) and perfused through the heart with a teleost Ringer solution followed by a fixative, consisting of 4% paraformaldehyde in 0.1 M phosphate buffer. The brains were postfixed for 12–24 h, cryoprotected with 30% sucrose, and sectioned at 60 mm on a cryostat. Sections were subsequently processed with an Alexa Fluor 488 Streptavidin complex (Jackson Immuno Research Laboratories; Antibody ID - AB_2337249; at 1:500) to label the biocytin filled cells, and DAPI (Sigma Aldrich # D9542; at 1:1000) and NeuroTrace 640 (ThermoFisher Scientific #N21483; at 1:500) to visualize the layers of ELL. Sections were then mounted on slides, dried of excess PBS, and coverslipped with either VectaShield Antifade (Vector Laboratories # H-1000-10) or Molecular Probes™ ProLong™ Diamond Antifade Mountant (Fisher Scientific; Molecular Probes™ P36965). Morphologically recovered neurons were inspected and subsequently photographed using a confocal microscope (Inverted Nikon A1R point-scanning laser confocal microscope with high-sensitivity GaAsP detectors) with either a 20× air objective or a 40× oil immersion objective. Images were collapsed along the Z-dimension implementing the maximum brightness per pixel. Each fluorescence channel was pseudo-colored as specified in Figure 2.

Modeling

Circuit architecture: The circuit consisted of one model granular cell receiving input from a small number (4 used in the main results, 4–7 tested in supplemental) of simulated afferents and one simulated inhibitory input.

Model granular cell: Each model granular cell is described by a single compartment with a membrane potential that evolves according to:

$$\frac{dV}{dt} = \frac{(I_L + I_E + I_I)}{C_M}$$

Membrane capacitance (C_M) values were chosen such that the model EPSP evoked by a single presynaptic input matched near threshold electrosensory responses of DGCs and SGCs (Figure S4). These values were 6 pF for DGCs and 12 pF for SGCs. The leak current (I_L) is described by:

$$I_L = g_L \times (v - E_L)$$

where v is the membrane potential of the model granular cell, the leak conductance g_L = 1 nS and the reversal potential E_L = −70 mV. These values were consistent with a prior *in vitro* study of ELL granular cells (Zhang et al., 2007).

Model synapse: Each synaptic current (I_E and I_I) is described by the standard equation:

$$I_{syn} = g_{syn} \times (v - E_{syn})$$

where the reversal potential of the excitatory conductance is 0 mV and the reversal potential of the inhibitory conductance is −90 mV. The timecourse of the excitatory conductance (g_E) follows a double exponential with a rise time constant τ_{E1} = 4 msec and a decay time constant τ_{E2} = 1 ms. The conductance parameter 's' is increased by w_e upon a spike event in a presynaptic electrosensory afferent and decays exponentially with time constant τ_{E2}. The excitatory conductance then evolves according to:

$$\frac{dg_E}{dt} = \frac{(invpeak \times s - g_E)}{\tau_{E1}}$$

where

$$invpeak = \left(\frac{\tau_{E2}}{\tau_{E1}}\right)^{\frac{\tau_{E1}}{(\tau_{E2} - \tau_{E1})}}$$

The inhibitory conductance (g_I) is increased by w_I upon a spike event in the stimulated presynaptic LMI and decays exponentially with time constant τ_I = 5 ms.

Electrosensory afferent (EA) input: For each model granular cell, a set of 4 EA inputs were either subsampled from recorded afferent data or simulated. The main results were not affected by the exact number of EA inputs to each model granular cell (Figure S4), for values within a plausible range based on past studies of the ELL (Bell, 1990a; Bell et al., 2005; Zhang et al., 2007). We simulated afferents by first calculating an exponential tuning curve of first spike latency versus stimulus amplitude. We randomly selected each set of exponential fit parameters from a multivariate Gaussian distribution that was fit to the recorded afferent data (Figures 4E–4G). We then added multiple spikes according to the mean spike offsets calculated in recorded EAs (Figure 4I). We constructed three different EA input conditions to separately test the effects of diverse latency tuning and diverse spike tuning and the combined effect of both (Figure 5E). To test the effect of diverse latency tuning on model granular cell responses (purple in Figures 5E–5H), we constructed a model EA tuning curve using the afferent population mean value for each latency tuning parameter, which was held constant, and added subsequent spikes with an offset determined by the recorded EA data (Figure 4I). We then randomly selected spike count tuning from recorded EAs to mask spikes in the latency tuning curve. To test the effect of diverse spike count tuning on granular cell responses (orange in Figures 5E–5H), we constructed model EA tuning curves by randomly selecting each set of exponential fit parameters from a multivariate Gaussian distribution that was fit to the recorded afferent data. We then added subsequent spikes with an offset determined by the recorded EA data (Figure 4I). Spikes were cutoff after a maximum spike latency calculated from the recorded EA data (11 ms). To test both diverse latency and spike count tuning (blue in Figures 5E–5H), we constructed a model EA tuning curve using the afferent population mean value for each latency tuning

parameter, which was held constant, and added subsequent spikes with an offset determined by the recorded EA data (Figure 4I). Spikes were cutoff after a maximum spike latency calculated from the recorded EA data (11 ms).

LMI inhibitory input: We simulated electrosensory-evoked inhibitory input to the model by specifying an input spike time with a constant onset latency relative to the earliest simulated EA input spike (we tested a range of onset latency from 2–5 msec; Figure S4). The weight of the inhibitory synapse (w_I) was varied as a sigmoid function of the membrane potential of the post-synaptic granular cell (v) at the time of the LMI spike, which provided a nice fit to the data (Figures 5C and 5D). This is meant to approximate the proposed ephaptic mechanism of LMI recruitment suggested by prior work (Han et al., 2000; Meek et al., 2001). However, equivalent results were obtained if the strength of inhibitory input was held constant as long as it was strong enough to truncate the response and suppress its normal peak.

Model simulation: All simulations were done in Python 3 with the BRIAN 2 simulator package (Stimberg et al., 2019). The model had a time step of 0.1 msec and was simulated for 50 msec in response to each electrosensory stimulus. Model GC responses were then quantified by measuring the peak membrane potential as was done for the real GCs recorded in this study. Each model cell was a simulation with a different EA input population.

QUANTIFICATION AND STATISTICAL ANALYSIS

Data were processed and analyzed offline using Python 3. Biophysical models were simulated and analyzed using the BRIAN 2 simulator package in Python 3 (Stimberg et al., 2019) (as noted above). No statistical methods were used to predetermine sample size. The experimenters were not blinded to the condition during data collection or analysis. Statistical test identity is indicated along with each result. Differences were considered significant at $p < 0.05$.

Supplementary Material

Refer to Web version on PubMed Central for supplementary material.

ACKNOWLEDGMENTS

This work was supported by grants from the NIH (NS075023 & NS118448), NSF (IOS-1656354) and Irma T. Hirschl Trust to N.B.S. and a Simons Foundation of Fellows Junior Fellowship to K.E.P. We thank C. Bell and A. Wallach for helpful discussions, L.F. Abbott for discussions and comments on the manuscript, and Federico Pedraja for assistance with Figure 1.

REFERENCES

Ashida G, and Carr CE (2011). Sound localization: jeffress and beyond. Curr. Opin. Neurobiol 21, 745–751. [PubMed: 21646012]

Bacelo J, Engelmann J, Hollmann M, von der EG, and Grant K (2008). Functional foveae in an electrosensory system. J. Comp. Neurol 511, 342–359. [PubMed: 18803238]

Bale MR, Davies K, Freeman OJ, Ince RA, and Petersen RS (2013). Low-dimensional sensory feature representation by trigeminal primary afferents. J. Neurosci 33, 12003–12012. [PubMed: 23864687]

Bathellier B, Buhl DL, Accolla R, and Carleton A (2008). Dynamic ensemble odor coding in the mammalian olfactory bulb: sensory information at different timescales. Neuron 57, 586–598. [PubMed: 18304487]

Bell C, and von der Emde G (1995). Electric organ corollary discharge pathways in mormyrid fish: II. The medial juxtalobar nucleus. J. Comp. Physiol. A 177, 463–479.

Bell CC (1989). Sensory coding and corollary discharge effects in mormyrid electric fish. J. Exp. Biol 146, 229–253. [PubMed: 2689564]

Bell CC (1990a). Mormyromast electroreceptor organs and their afferents in mormyrid electric fish: II. Intra-axonal recordings show initial stages of central processing. J. Neurophysiol 63, 303–318. [PubMed: 2313347]

Bell CC (1990b). Mormyromast electroreceptor organs and their afferents in mormyrid electric fish: III. Physiological differences between two morphological types of fibers. J. Neurophysiol 63, 319–332. [PubMed: 2313348]

Bell CC, Grant K, and Serrier J (1992). Corollary discharge effects and sensory processing in the mormyrid electrosensory lobe: I. Field potentials and cellular activity in associated structures. J. Neurophysiol 68, 843–858. [PubMed: 1432052]

Bell CC, Meek J, and Yang JY (2005). Immunocytochemical identification of cell types in the mormyrid electrosensory lobe. J. Comp. Neurol 483, 124–142. [PubMed: 15672392]

Bell CC, Zakon H, and Finger TE (1989). Mormyromast electroreceptor organs and their afferent fibers in mormyrid fish: I. Morphology. J. Comp. Neurol 286, 391–407. [PubMed: 2768566]

Brasselet R, Panzeri S, Logothetis NK, and Kayser C (2012). Neurons with stereotyped and rapid responses provide a reference frame for relative temporal coding in primate auditory cortex. J. Neurosci 32, 2998–3008. [PubMed: 22378873]

Chase SM, and Young ED (2007). First-spike latency information in single neurons increases when referenced to population onset. Proc. Natl. Acad. Sci. U S A 104, 5175–5180. [PubMed: 17360369]

Chen L, House JL, Krahe R, and Nelson ME (2005). Modeling signal and background components of electrosensory scenes. J. Comp. Physiol. A. Neuroethol Sens Neural Behav. Physiol 191, 331–345. [PubMed: 15800793]

Chong E, Moroni M, Wilson C, Shoham S, Panzeri S, and Rinberg D (2020). Manipulating synthetic optogenetic odors reveals the coding logic of olfactory perception. Science 368, eaba2357. [PubMed: 32554567]

Chong E, and Rinberg D (2018). Behavioral readout of spatio-temporal codes in olfaction. Curr. Opin. Neurobiol 52, 18–24. [PubMed: 29694923]

Crapse TB, and Sommer MA (2008). Corollary discharge across the animal kingdom. Nat. Rev. Neurosci 9, 587–600. [PubMed: 18641666]

Cury KM, and Uchida N (2010). Robust odor coding via inhalation-coupled transient activity in the mammalian olfactory bulb. Neuron 68, 570–585. [PubMed: 21040855]

Furukawa S, and Middlebrooks JC (2002). Cortical representation of auditory space: information-bearing features of spike patterns. J. Neurophysiol 87, 1749–1762. [PubMed: 11929896]

Gawne TJ, Kjaer TW, and Richmond BJ (1996). Latency: another potential code for feature binding in striate cortex. J. Neurophysiol 76, 1356–1360. [PubMed: 8871243]

Goldberg JM (2000). Afferent diversity and the organization of central vestibular pathways. Exp. Brain Res 130, 277–297. [PubMed: 10706428]

Gollisch T, and Meister M (2008). Rapid neural coding in the retina with relative spike latencies. Science 319, 1108–1111. [PubMed: 18292344]

Gomez L, Budelli R, Grant K, and Caputi AA (2004). Pre-receptor profile of sensory images and primary afferent neuronal representation in the mormyrid electrosensory system. J. Exp. Biol 207, 2443–2453. [PubMed: 15184516]

Gottwald M, Singh N, Haubrich AN, Regett S, and von der Emde G (2018). Electric-color sensing in weakly electric fish suggests color perception as a sensory concept beyond vision. Curr. Biol 28, 3648–3653.e3642. [PubMed: 30416061]

Grant K, Meek J, Sugawara Y, Veron M, Denizot JP, Hafmans J, Serrier J, and Szabo T (1996). Projection neurons of the mormyrid electrosensory lateral line lobe:morphology, immunocytochemistry and synaptology. J. Comp. Neurol 375, 18–42. [PubMed: 8913891]

Grant K, Sugawara S, Gomez L, Han VZ, and Bell CC (1998). The mormyrid electrosensory lobe *in vitro*: physiology and pharmacology of cells and circuits. J. Neurosci 18, 6009–6025. [PubMed: 9671686]

Grothe B (2003). New roles for synaptic inhibition in sound localization. Nat. Rev. Neurosci 4, 540–550. [PubMed: 12838329]

Grothe B, and Klump GM (2000). Temporal processing in sensory systems. Curr. Opin. Neurobiol 10, 467–473. [PubMed: 10981615]

Gutig R, and Sompolinsky H (2006). The tempotron: a neuron that learns spike timing-based decisions. Nat. Neurosci 9, 420–428. [PubMed: 16474393]

Haddad R, Lanjuin A, Madisen L, Zeng H, Murthy VN, and Uchida N (2013). Olfactory cortical neurons read out a relative time code in the olfactory bulb. Nat. Neurosci 16, 949–957. [PubMed: 23685720]

Hall JC, Bell C, and Zelick R (1995). Behavioral evidence of a latency code for stimulus intensity in mormyrid electric fish. J. Comp. Physiol. A, 29–39.

Han VZ, Grant K, and Bell CC (2000). Rapid activation of GABAergic interneurons and possible calcium independent GABA release in the mormyrid elelctrosensory lobe. J. Neurophysiol 83, 1592–1604. [PubMed: 10712482]

Heil P (2004). First-spike latency of auditory neurons revisited. Curr. Opin. Neurobiol 14, 461–467. [PubMed: 15321067]

Hollmann V, Engelmann J, and Gomez-Sena L (2016). A quest for excitation: theoretical arguments and immunohistochemical evidence of excitatory granular cells in the ELL of Gnathonemus petersii. J. Physiol. Paris 110, 190–199. [PubMed: 27815181]

Johansson RS, and Birznieks I (2004). First spikes in ensembles of human tactile afferents code complex spatial fingertip events. Nat. Neurosci 7, 170–177. [PubMed: 14730306]

Kennedy A, Wayne G, Kaifosh P, Alvina K, Abbott LF, and Sawtell NB (2014). A temporal basis for predicting the sensory consequences of motor commands in an electric fish. Nat. Neurosci 17, 416–422. [PubMed: 24531306]

Lennie P (2003). The cost of cortical computation. Curr. Biol 13, 493–497. [PubMed: 12646132]

Liberman MC (1982). Single-neuron labeling in the cat auditory nerve. Science 216, 1239–1240. [PubMed: 7079757]

Liberman MC, and Oliver ME (1984). Morphometry of intracellularly labeled neurons of the auditory nerve: correlations with functional properties. J. Comp. Neurol 223, 163–176. [PubMed: 6200517]

Lyons-Warren AM, Kohashi T, Mennerick S, and Carlson BA (2013). Detection of submillisecond spike timing differences based on delay-line anticoincidence detection. J. Neurophysiol 110, 2295–2311. [PubMed: 23966672]

Meek J, Grant K, and Bell C (1999). Structural organization of the mormyrid electrosensory lateral line lobe. J. Exp. Biol 202, 1291–1300. [PubMed: 10210669]

Meek J, Hafmans TGM, Han VZ, Bell CC, and Grant K (2001). Myelinated dendrites in the mormyrid electrosensory lobe. J. Comp. Neurol 431, 255–275. [PubMed: 11170004]

Meyer JH, and Bell CC (1983). Behavioral measurements of sensory gating by a corollary discharge. J. Comp. Physiol 151, 401–406.

Mohr C, Roberts PD, and Bell CC (2003). The mormyromast region of the mormyrid electrosensory lobe. II. Responses to input from central sources. J. Neurophysiol 90, 1211–1223. [PubMed: 12904506]

Moore JD, Deschenes M, Furuta T, Huber D, Smear MC, Demers M, and Kleinfeld D (2013). Hierarchy of orofacial rhythms revealed through whisking and breathing. Nature 497, 205–210. [PubMed: 23624373]

Panzeri S, Ince RA, Diamond ME, and Kayser C (2014). Reading spike timing without a clock: intrinsic decoding of spike trains. Philos. Trans. R. Soc. Lond. B Biol. Sci 369, 20120467. [PubMed: 24446501]

Panzeri S, Petersen RS, Schultz SR, Lebedev M, and Diamond ME (2001). The role of spike timing in the coding of stimulus location in rat somatosensory cortex. Neuron 29, 769–777. [PubMed: 11301035]

Petitpre C, Wu H, Sharma A, Tokarska A, Fontanet P, Wang Y, Helmbacher F, Yackle K, Silberberg G, Hadjab S, et al. (2018). Neuronal heterogeneity and stereotyped connectivity in the auditory afferent system. Nat. Commun 9, 3691. [PubMed: 30209249]

Raman B, Joseph J, Tang J, and Stopfer M (2010). Temporally diverse firing patterns in olfactory receptor neurons underlie spatiotemporal neural codes for odors. J. Neurosci 30, 1994–2006. [PubMed: 20147528]

Rieke F, warland D, Steveninck R.R.d.R.v., and Bialek W (1996). Spikes Exploring the Neural Code (MIT Press).

Russell CJ, Myers JP, and Bell CC (1974). The echo response in Gnathonemus petersii. J. Comp. Physiol 92, 181–200.

Saal HP, Wang X, and Bensmaia SJ (2016). Importance of spike timing in touch: an analogy with hearing? Curr. Opin. Neurobiol 40, 142–149. [PubMed: 27504741]

Sawtell NB (2010). Multimodal integration in granule cells as a basis for associative plasticity and sensory prediction in a cerebellum-like circuit. Neuron 66, 573–584. [PubMed: 20510861]

Sawtell NB, and Williams A (2008). Transformations of electrosensory encoding associated with an adaptive filter. J. Neurosci 28, 1598–1612. [PubMed: 18272681]

Sawtell NB, Williams A, Roberts PD, and von der Emde G (2006). Effects of sensing behavior on a latency code. J. Neurosci 26, 8221–8234. [PubMed: 16899717]

Shusterman R, Smear MC, Koulakov AA, and Rinberg D (2011). Precise olfactory responses tile the sniff cycle. Nat. Neurosci 14, 1039–1044. [PubMed: 21765422]

Smear M, Shusterman R, O'Connor R, Bozza T, and Rinberg D (2011). Perception of sniff phase in mouse olfaction. Nature 479, 397–400. [PubMed: 21993623]

Stanley GB (2013). Reading and writing the neural code. Nat. Neurosci 16, 259–263. [PubMed: 23434978]

Stern M, Bolding KA, Abbott LF, and Franks KM (2018). A transformation from temporal to ensemble coding in a model of piriform cortex. Elife 7, e34831. [PubMed: 29595470]

Stimberg M, Brette R, and Goodman DF (2019). Brian 2, an intuitive and efficient neural simulator. Elife 8, e47314. [PubMed: 31429824]

Szabo T, and Hagiwara S (1967). A latency-change mechanism involved in sensory coding of electric fish (mormyrids). Physiol. Behav 2, 331–335.

Theunissen F, and Miller JP (1995). Temporal encoding in nervous systems: a rigorous definition. J. Comput. Neurosci 2, 149–162. [PubMed: 8521284]

Thomson EE, and Kristan WB (2006). Encoding and decoding touch location in the leech CNS. J. Neurosci 26, 8009–8016. [PubMed: 16870746]

Thorpe S, Delorme A, and Van Rullen R (2001). Spike-based strategies for rapid processing. Neural Netw. 14, 715–725. [PubMed: 11665765]

Uchida N, Poo C, and Haddad R (2014). Coding and transformations in the olfactory system. Annu. Rev. Neurosci 37, 363–385. [PubMed: 24905594]

VanRullen R, Guyonneau R, and Thorpe SJ (2005). Spike times make sense. Trends Neurosci. 28, 1–4. [PubMed: 15626490]

Viemeister NF (1983). Auditory intensity discrimination at high frequencies in the presence of noise. Science 221, 1206–1208. [PubMed: 6612337]

von der Emde G, and Bleckmann H (1992). Differential responses of two types of electroreceptive afferents to signal distortions may permit capacitance measurement in a weakly electric fish, _Gnathonemus petersii_. J. Comp. Physiol. A 171, 683–694.

von der Emde G, and Bleckmann H (1997). Waveform tuning of electroreceptor cells in the weakly electric fish, *Gnathonemus petersii*. J. Comp. Physiol. A 181, 511–524.

Winter IM, Robertson D, and Yates GK (1990). Diversity of characteristic frequency rate-intensity functions in guinea pig auditory nerve fibres. Hear Res. 45, 191–202. [PubMed: 2358413]

Zhang J, Han VZ, Meek J, and Bell CC (2007). Granular cells of the mormyrid electrosensory lobe and postsynaptic control over presynaptic spike occurrence and amplitude through an electrical synapse. J. Neurophysiol 97, 2191–2203. [PubMed: 17229820]

Zohar O, Shackleton TM, Nelken I, Palmer AR, and Shamir M (2011). First spike latency code for interaural phase difference discrimination in the guinea pig inferior colliculus. J. Neurosci 31, 9192–9204. [PubMed: 21697370]

Zohar O, and Shamir M (2016). A readout mechanism for latency codes. Front Comput. Neurosci 10, 107. [PubMed: 27812332]

Highlights

- Spike latency is transformed into graded changes in postsynaptic response amplitude
- Motor corollary discharge signals are not required for decoding spike latency
- Diverse receptor tuning and rapid inhibition play key roles in decoding spike latency

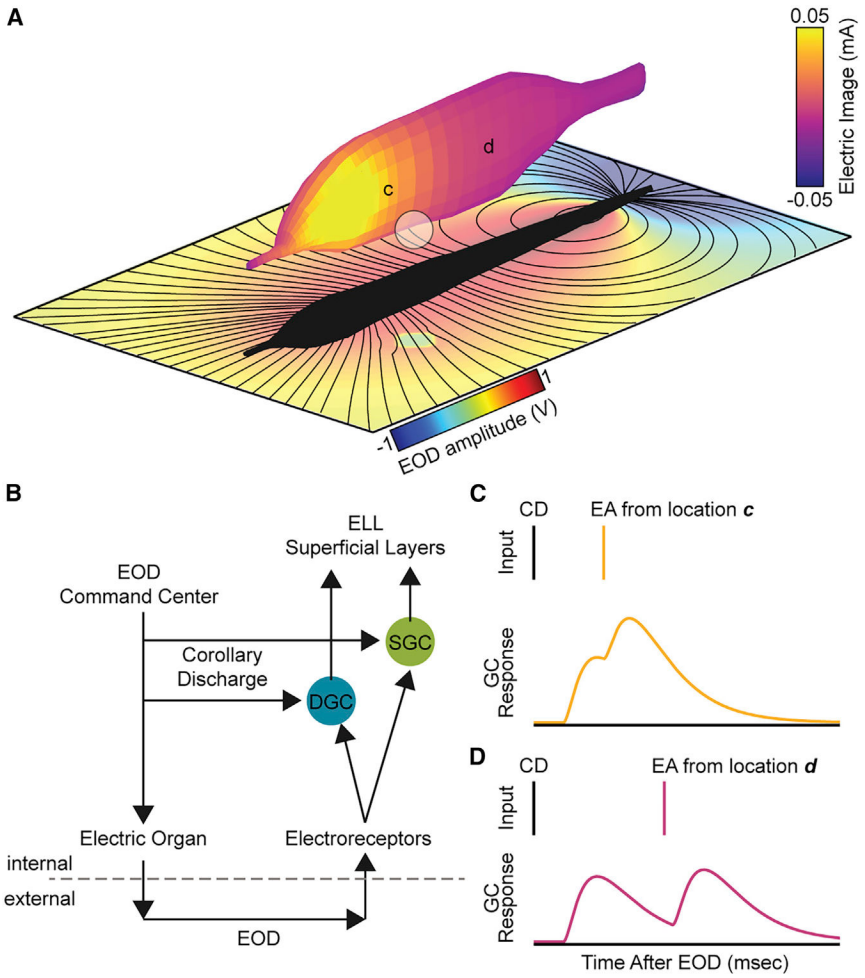

Figure 1. Central readout of a latency code for electrosensory stimulus amplitude based on corollary discharge

(A) Weakly electric mormyrid fish emit brief pulses of electricity known as electric organ discharges (EODs; bottom plane). Nearby objects induce “electrical images” on the body surface by changing local current density (amplitude) of the resulting electric field. Electrical image amplitude is encoded by the latency and number of spikes fired by afferent fibers innervating electroreceptors on the skin (EAs). Increased electric image amplitude yields decreased EA spike latency and increased EA spike number.

(B) Two distinct classes of granular cells in the electrosensory lobe—superficial (SGC; green) and deep (DGC; teal)—integrate excitatory input from EAs with a centrally originating corollary discharge (CD) input related to the motor command to discharge the electric organ.

(C) Latency coded information is hypothesized to be read out in granular cells (GCs) based on summation of EA input (yellow line) with a fixed temporal reference signal provided by CD (black line). In such a scheme, a short-latency EA spike arriving near the peak of the CD-evoked depolarization (yellow) would yield a larger amplitude granular cell postsynaptic response. EA receptive field location is shown on the body surface in (A).

(D) Same as in (C), but for a longer latency EA spike (purple) arriving on the falling phase of the depolarization evoked by CD input (black line), which yields a smaller amplitude granular cell postsynaptic response than in (C).

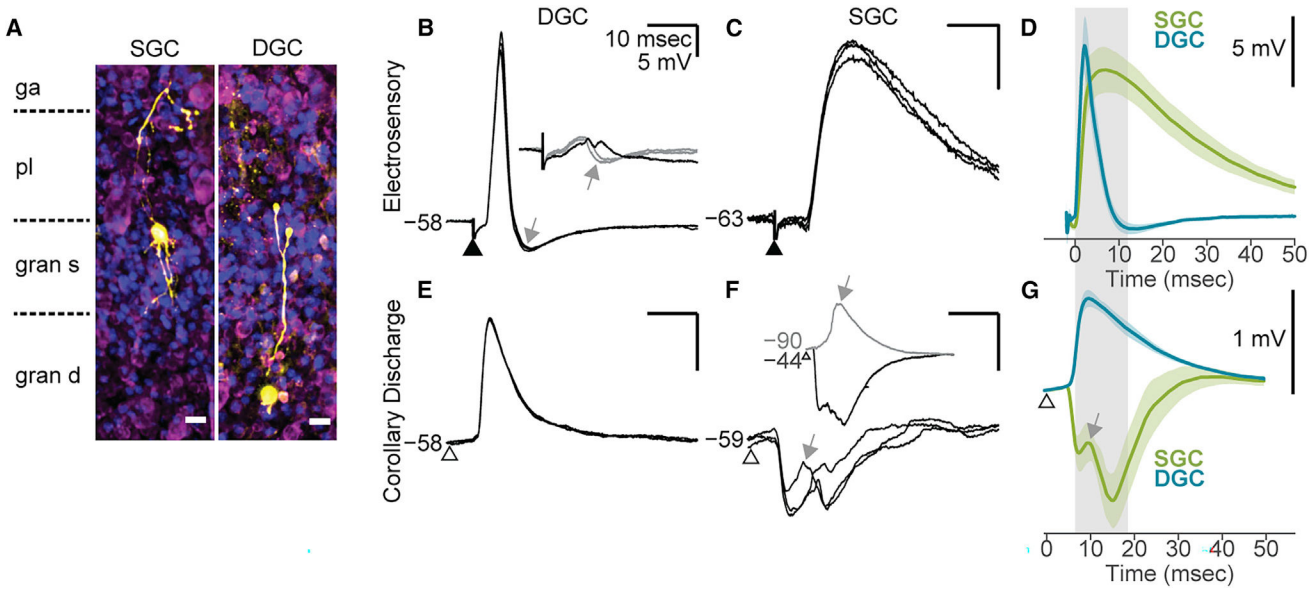

Figure 2. Responses of granular cells to electrosensory and corollary discharge inputs

(A) Confocal z stacks of an SGC and a DGC labeled with biocytin (yellow) during whole-cell recording. DAPI (blue) and Neurotrace (magenta) staining show the layers of the ELL. Scale bar, 10 μm (gang, ganglion layer; plex, plexiform layer; gran s, superficial granular cell layer; gran d, deep granular cell layer).

(B) Example DGC response to electrosensory input (three trials overlaid) aligned to stimulus onset (solid arrowhead). Baseline membrane potential was −58 mV. The rapid decay of the EPSP is likely due to synaptic inhibition (gray arrow). Inset: three trials overlaid in response to a weaker electrosensory stimulus at threshold for evoking an IPSP (gray arrow) that truncates the electrosensory-evoked EPSP. The black trace shows a trial in which the EPSP occurred in the absence of the IPSP.

(C) Example SGC response to electrosensory input (three trials overlaid) aligned to stimulus onset (solid arrowhead). Baseline membrane potential was −63 mV.

(D) Average response of DGCs (teal, n = 24) and SGCs (green, n = 18) to the electrosensory stimulus. Responses aligned to the EPSP onset (time = 0) to average across cells. Shading denotes SEM. DGC responses (n = 24) peaked earlier (2.5 ± 1 ms versus 11 ± 8.2 ms; $t(42) = -4.99$, $p < 0.001$), decayed more rapidly (2.6 ± 1.3 ms versus 33.3 ± 32.8 ms; $t(42) = -4.61$, $p < 0.001$), and were narrower (half-width at half-height 3.6 ± 1.7 ms versus 24.8 ± 11.4 ms; $t(42) = -9.04$, $p < 0.001$) than those of SGCs (n = 18).

(E) Example DGC response to electric organ corollary discharge (CD) input (three repeated trials overlaid). Open arrowhead indicates the time of the EOD motor command recorded by an electrode near the electric organ.

(F) Example SGC response to CD input (three repeated trials overlaid). Inset: CD response for a different SGC illustrating an excitatory response (gray arrow) evident at a hyperpolarized membrane potential near reversal for the inhibitory response in this cell (gray; trial average). At a depolarized membrane potential (black; trial average), this cell showed rapid, early onset inhibition followed by a depolarizing deflection (gray arrow). Open arrowheads indicate the time of the EOD motor command.

(G) Average CD responses across a subset of DGCs (teal; n = 5) and SGCs (green; n = 5) selected for their similar resting membrane potentials (−50 to −60 mV). Shading denotes SEM. Open arrowhead indicates the time of the EOD motor command. Gray boxed region indicates the range of latency shifts observed in EAs (6.5–18.5 ms), shown relative to the timing of granular cell CD responses. CD input evoked short-latency EPSPs in DGCs (onset 5.7 ± 0.8 ms; peak 9.7 ± 2.7 ms, n = 24) and even shorter latency IPSPs in SGCs (4.9 ± 0.5 ms, n = 12). A depolarizing PSP was observed after inhibition onset (gray arrow; onset 7.6 ± 2.2 ms; peak 14.4 ± 5.8 ms) in 12/18 SGCs. In 3/24 DGCs, we observed a prominent IPSP at around 7.7 ms. See also Figure S1.

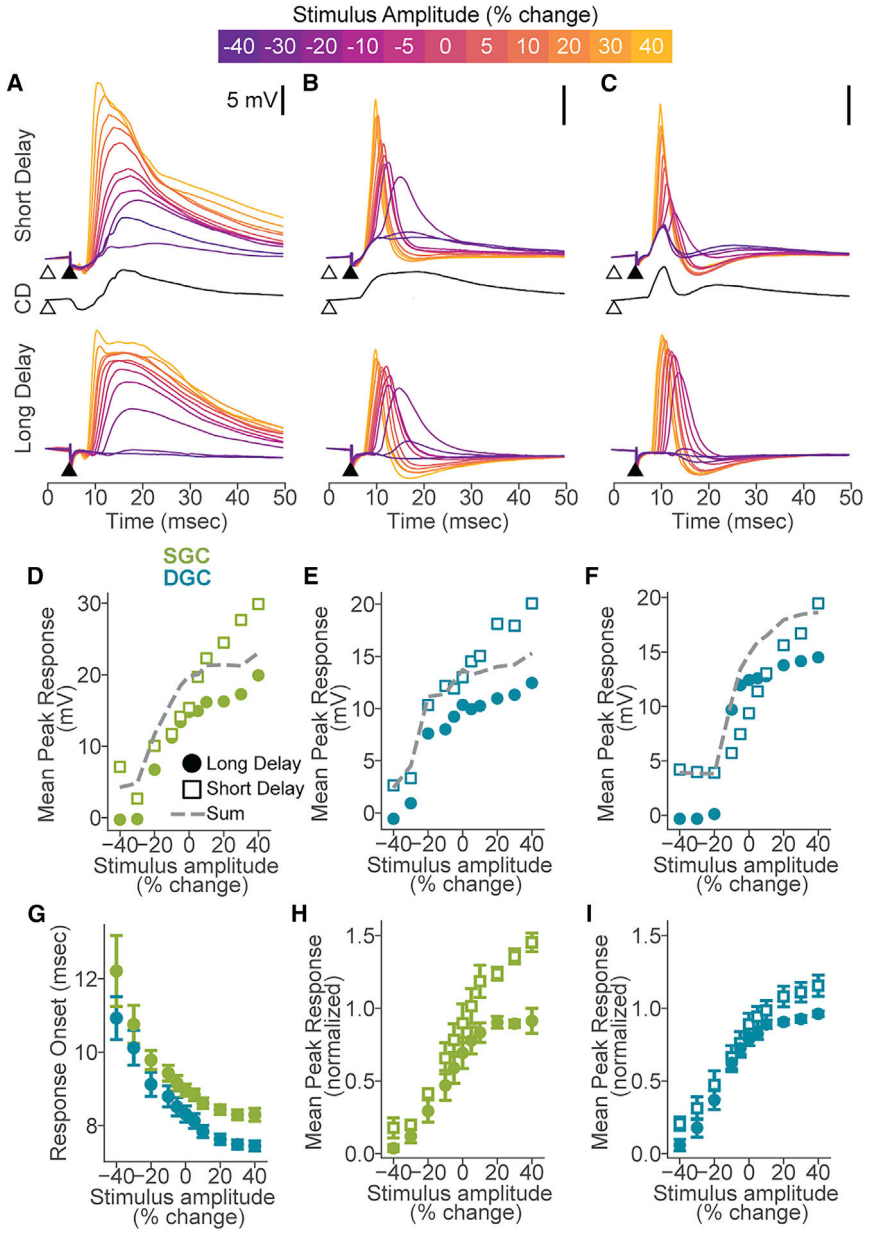

Figure 3. Corollary discharge enhances but is not required for electrosensory responses in granular cells

(A) Responses of an example SGC across amplitudes (color bar, top) to stimuli delivered either at a short (top) or long (bottom) delay relative to the EOD motor command. Middle: average response to corollary discharge (CD) input alone. Solid arrowhead indicates time of the electrosensory stimulus. Open arrowhead indicates the time of the EOD command.

(B and C) Same displays as in (A), but for two example DGCs.

(D) Mean peak response versus stimulus amplitude for the same SGC shown in (A) in long delay (filled circle) versus short delay (open square) conditions. The predicted response at a short delay ("sum," gray dashed) was calculated by adding the long delay response at each stimulus amplitude to the CD response.

(E and F) Same displays as in (D) but for the example DGCs shown in (B) and (C).

(G) Response onset latency (relative to stimulus onset at a long delay relative to the CD; mean ± SEM) versus stimulus amplitude for SGCs (green; n = 5) and DGCs (teal; n = 13). (H) Peak response amplitude versus stimulus amplitude under long delay (filled circle) versus short delay (open square) conditions for SGCs (n = 5; mean ± SEM). Responses within each cell were normalized by the maximum long delay response amplitude before averaging across cells. The delay between the electrosensory stimulus and the command had a significant effect on peak response amplitude, $F(1,88) = 55$, $P < 0.001$ (two-factor repeated measures ANOVA). Across the range of −10 to 10% stimulus amplitude, the sensitivity at a long delay was 8.3 ± 5.6 mV, and the sensitivity increased to 27.9 ± 8.8 mV at a short delay. Out of four SGCs with at least five trials in every condition, all had a significant effect of stimulus delay on raw peak response amplitude ($p < 0.001$). (I) Same as in (H), but for DGCs (n = 13; mean ± SEM). The delay between the electrosensory stimulus and the command had a significant effect on peak response amplitude, $F(1, 264) = 21$, $p < 0.001$ (two-factor repeated measures ANOVA). Across the range of −10 to 10% stimulus amplitude, the sensitivity at a long delay was 8.1 ± 8.1 mV, and the sensitivity increased to 26.8 ± 14.6 mV at a short delay. Out of nine DGCs with at least five trials in every condition, seven had a significant effect of stimulus delay on raw peak response amplitude ($p <= 0.001$).

(H and I) Significant effects of stimulus amplitude and delay, but not delay-by-amplitude interaction at $p < 0.001$ on the mean peak response amplitudes across cells. See also Figures S2 and S3.

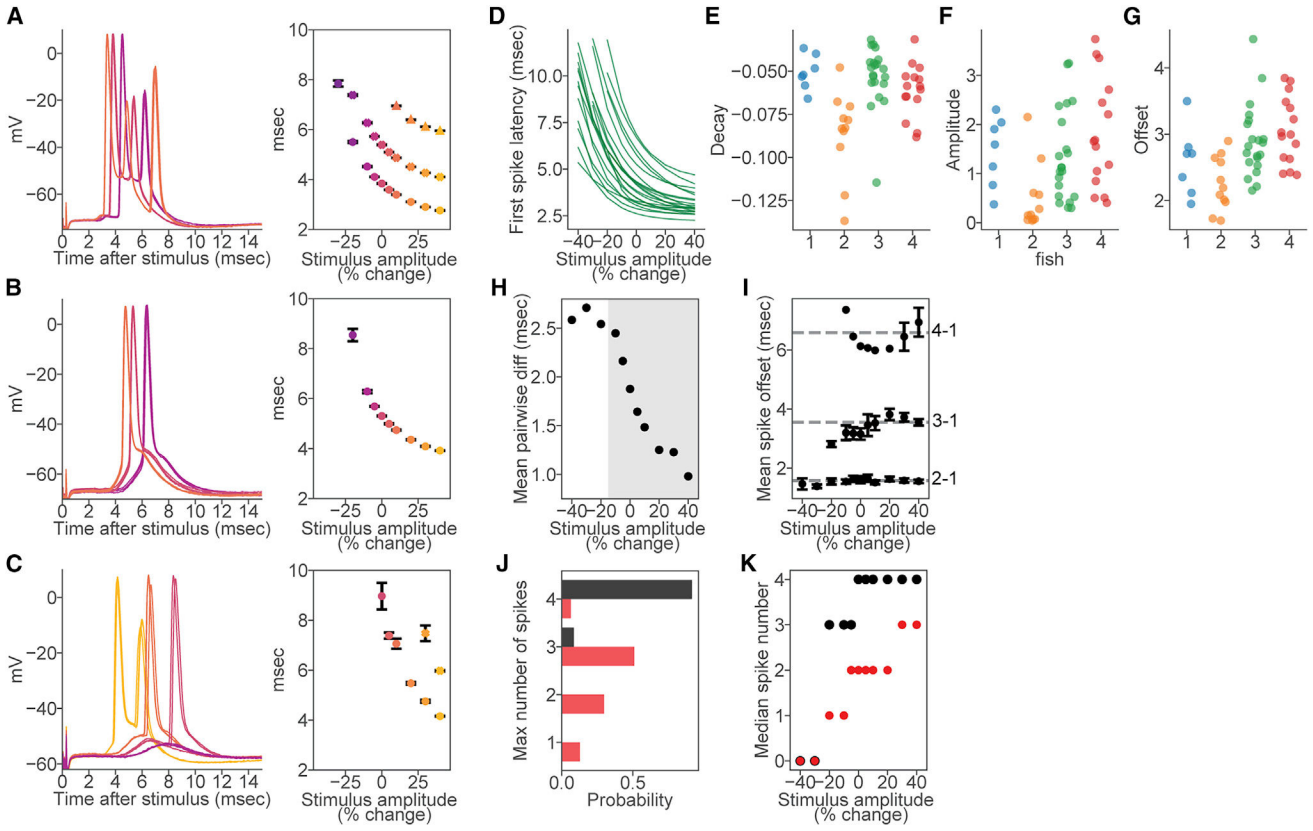

Figure 4. Electroreceptor afferents exhibit diverse first spike latency and spike count tuning

(A) Left: intracellular responses of a recorded EA at stimulus amplitudes of −10, 0, and +10% (colored according to the scatterplot at right). Three trials overlaid at each amplitude. Right: spike latency versus stimulus amplitude (mean ± SEM).

(B and C) Same as (A), but for two other example EAs with notable differences in latency and spike count tuning. In (C), three trials at +40% amplitude are also shown.

(D) Exponential fits of first spike latencies across stimulus amplitudes for 21 electroreceptor afferents recorded from a single fish (fish 3 in E–G).

(E–G) Heterogeneity of fit parameters among EAs recorded in four fish (n = 7, 11, 21, 15 EAs per fish).

(H) Mean pairwise latency among first spikes (n = 58 total EAs in four fish). Shading denotes stimulus range for which >94% of EAs have at least one spike.

(I) Scatterplot of spike offset (mean ± SEM) for second (1.6 ± 0.5 ms, n = 360 spikes), third (3.6 ± 0.8 ms, n = 145 spikes), and fourth (6.6 ± 0.8 ms, n = 13 spikes) spikes relative to first spike latency. For each datapoint (mean ± SEM), EAs without that spike number were ignored.

(J) Probability of EAs having zero, one, two, three, or four spikes at the maximum stimulus amplitude (+40%) for recorded data (red) and the prediction (black) based on recorded first spike latency and mean spike offsets, as in (I) (n = 58 EAs).

(K) Median number of spikes per EAs across stimulus amplitude for actual (red) and predicted (black) spikes (n = 58 EAs).

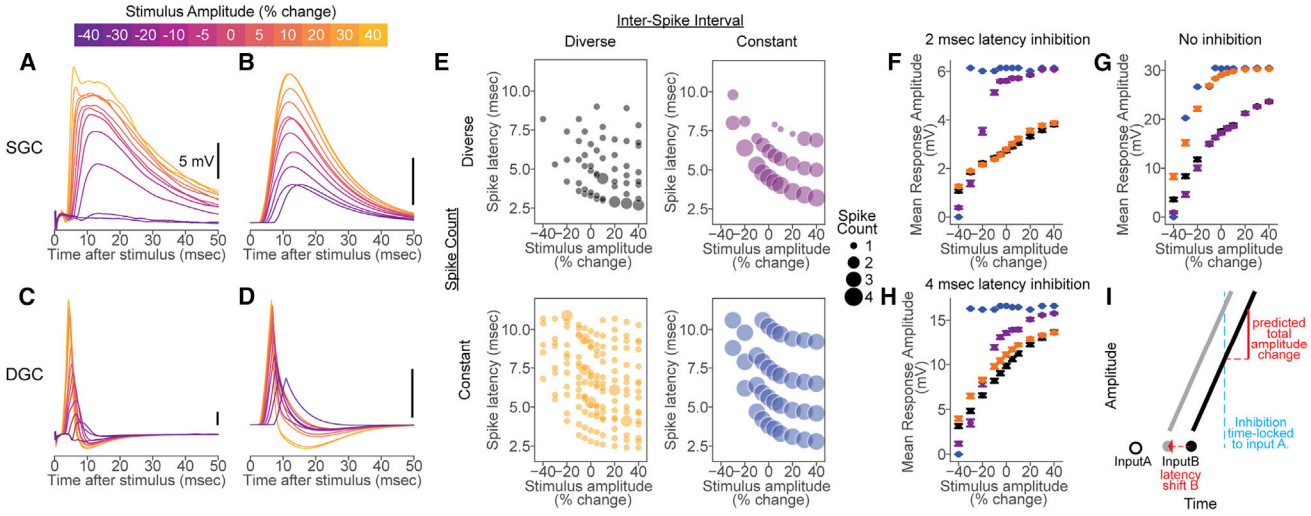

Figure 5. Summation of diversely tuned EAs accounts for graded readout of stimulus amplitude in granular cells

(A) Responses of an example SGC to electrosensory stimuli of different amplitudes (color bar, top) delivered at a long delay from CD input.

(B) Example responses of a model granular cell receiving four excitatory EA inputs.

(C) Responses of an example DGC to electrosensory stimuli of different amplitudes delivered at a long delay from CD input.

(D) Example responses of a model granular cell with the same excitatory EA input as in (B), but with an inhibitory conductance driven by the first spike in the EA input population, at a 4-ms delay.

(E) Examples of four sets of EA population inputs (n = 4 EAs per population) designed to test the effects of diverse latency (effecting the input inter-spike interval) and spike count tuning on granular cell responses (see main text). Circles denote the time of EA spikes with the size indicating the number of spikes. Black, subsampled recorded EA data. Orange, diverse latency tuning is preserved while diverse spike count tuning is removed. Purple, diverse latency tuning is removed while diverse spike count tuning is preserved. Blue, diverse latency and spike count tuning are both removed from the input population.

(F) Peak response amplitude versus stimulus amplitude across model DGCs (mean ± SEM; n = 200 different EA input populations) under each condition shown in

(E) with inhibition delayed by 2 ms relative to the first EA spike.

(G) Same as in (F), but for model SGCs.

(H) Same as in (F), but with inhibition delayed by 4 ms relative to the first EA spike.

(I) Shifts in a second EA input *B* relative to a first EA input *A* (dotted red arrow) cause a predictable change in the amplitude of the second EPSP when an inhibitory input (blue), time locked to input *A*, cuts off the response during the EPSP rise. The predicted response amplitude change (red, solid line) depends on the slope of the EPSP rise. See also Figure S4.

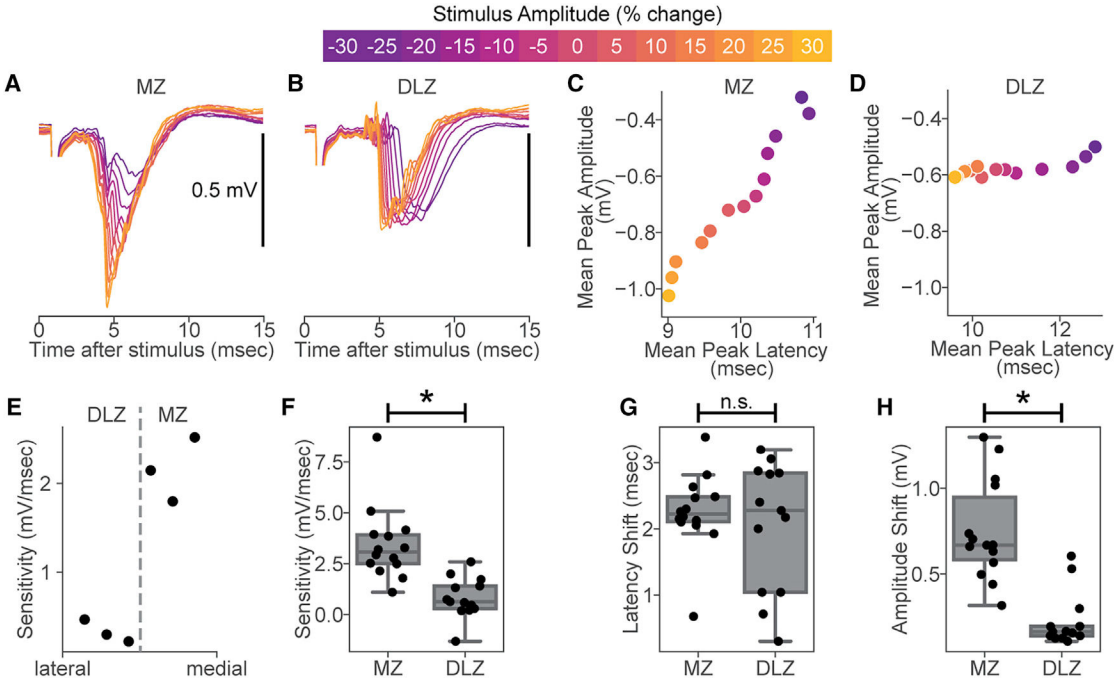

Figure 6. Differences in EA tuning variability result in different stimulus readouts in MZ and DLZ

(A) Local field potential (LFP) in the medial zone (MZ) of ELL in response to different stimulus amplitudes (color bar, top).

(B) Same as in (A), but for the dorsolateral done (DLZ).

(C) Scatterplot of LFP amplitude versus LFP peak latency relative to stimulus onset for MZ.

(D) Same as in (C), but for DLZ. Shifts in stimulus amplitude cause shifts in peak latency for both zones, but peak amplitude changes are greater in the MZ.

(E) Sensitivity of LFP amplitude to latency shifts for a series of closely spaced electrode penetrations at different mediolateral locations (spaced approximately 200 μm apart) spanning the MZ-DLZ border, as determined by shifts in receptive location on the skin. Note the abrupt jump in sensitivity around the zonal border.

(F) Sensitivity of LFP amplitude is greater in MZ compared with DLZ ($t(25) = 4.6$, $p < 0.001$; n = 14 MZ sites, n = 13 DLZ sites). Boxplots denote 25%, 50%, and 75% quartiles (with error bars denoting the rest of the distribution, excluding outliers). Sensitivity was calculated as the change in LFP amplitude (mV) divided by the change in LFP peak latency (ms) across the full range of stimulus amplitudes.

(G) LFP peak latency in MZ and DLZ shifts similar amounts (measured across the full stimulus amplitude range; $t(25) = 0.63$, $p = 0.53$; n = 14 MZ sites, n = 13 DLZ sites).

(H) LFP amplitude changes are greater in MZ versus DLZ (measured across the full stimulus amplitude range; $t(25) = 5.8$, $p < 0.001$; n = 14 MZ sites, n = 13 DLZ sites).

KEY RESOURCES TABLE

REAGENT or RESOURCE	SOURCE	IDENTIFIER
Antibodies		
Alexa Fluor 488 Streptavidin complex	Jackson Immuno Research Laboratories	RRID: AB_2337249
Chemicals, peptides, and recombinant proteins		
DAPI	Sigma Aldrich	D9542
NeuroTrace 640	ThermoFisher Scientific	N21483
Deposited data		
Full dataset (including raw and processed data and custom scripts)	This paper	Database: 10.12751/g-node.suibcf
Experimental models: Organisms/strains		
Gnathonemus petersii	AliKhan Tropical Fish	wild-caught and imported
Software and algorithms		
Python	https://anaconda.org/	V3.6.12
Brian2	https://briansimulator.org/	V2.3.0.2
Spike2	Cambridge Electronic Designs	v7